

SYNTHESIS OF 2D g-C₃N₄/BiOCl HETEROJUNCTION WITH MIXED SOLVENTS TO ENHANCE VISIBLE-LIGHT PHOTOCATALYTIC PERFORMANCE

Aung Khaing^{1,4}, Dong Yang^{2,3}, Yao Chen³, Zhongyi Jiang^{*4}

Abstract

Visible-light response and highly effective charge separation are the vital factors to improve the photocatalytic performance of photocatalysts. In this study, two-dimensional (2D) graphitic carbon nitride/bismuth oxychloride (g-C₃N₄/BiOCl) heterojunctions were synthesized by one-pot ethanol-assisted solvothermal process in the presence of ionic liquid 1-butyl-3-methyl imidazolium chloride ([Bmim]Cl). The ionic liquid acts as solvent, and electrically conducting fluids in the synthesis process, contributing to the uniform dispersion of g-C₃N₄ on the BiOCl surface. The nanostructured heterojunction was formed with g-C₃N₄ covering the surface of BiOCl nanosheets uniformly. 2D g-C₃N₄/BiOCl heterojunctions showed higher photocatalytic performance for Rhodamine B (RhB) under visible-light irradiation compared with pure g-C₃N₄ and BiOCl. The mechanism of synthesized sample g-C₃N₄/BiOCl-4 showed that [•]O²⁻ and h⁺ plays an active role in the degradation process and the separation of photo induced charges transversely the heterostructure boundary reversed electron-hole recombination. This study provides a new insight into the development of high efficient and stable catalyst with tunable catalytic activity.

Keywords: g-C₃N₄/BiOCl, heterojunction, photocatalyst, ionic liquid, Rhodamine B

Introduction

In recent years, there is an increasing interest in the study of photocatalysis technology applications for water/air purification (Fujishima *et al.*, 2000; Sharma *et al.*, 2015), hydrogen production (Yamasita *et al.*, 2004), self-cleaning coatings (Zhang *et al.*, 2005) and solar cells (Regan *et al.*, 1991). Taking advantage of inexhaustible solar energy as the driving source, the photocatalytic technology has been regarded as a “green” method to deal with environmental pollution and energy shortage alongside (Yan *et al.*, 2009). Recently, the varieties of inorganic semiconductors and molecular assemblies have been developed as photocatalysts under visible-light (Akhavan and Ghaderi, 2013; Weng *et al.*, 2013; Wang *et al.*, 2009; Hou *et al.*, 2014). However, most of them lack the ability of directly utilizing visible-light, which seriously hinders their further development in environment remediation.

Graphite-like carbon-nitride (g-C₃N₄), a metal-free photocatalyst has shown great photocatalytic performance due to its visible-light response (Kang *et al.*, 2013). Moreover, g-C₃N₄ is recognized to be the more stable derivative of carbon with high stability and moderate band gap of ~2.7 eV (Regan *et al.*, 1991). The most distinct feature of the layered g-C₃N₄ from other common layered compound is the presence of abundant hydrogen bonds, which dominate the intra-layered framework due to the incomplete polymerization of the precursors containing amine groups (Cai *et al.*, 2015). However, the photocatalytic performance of g-C₃N₄ is strongly hindered by the fast recombination of photogenerated electrons and holes in a very short time. Thus, several strategies such as constructing heterojunction structure, regulating surface morphology and compositing carbon material, have been applied to promote the separation efficiency of photogenerated carriers. Among them, constructing type II or Z-scheme heterojunction structure can effectively separate

¹ Lecturer, Department of Chemistry, University of Yangon

² Key Laboratory of System Bioengineering of Ministry of Education, School of Chemical Engineering and Technology, Tianjin University, 300072, China

³ School of Environmental Science and Engineering, Tianjin University, 300072, China

⁴ Collaborative Innovation Center of Chemical Science and Engineering (Tianjin), Tianjin 300072, China

* Corresponding author, Zhongyi Jiang, zhyjiang@tju.edu.cn Tel: +86-22-27406646

electrons and holes to different materials due to the inequality of energy bands. To date, a variety of metal composite materials have been utilized as the second component, in which the bismuth-based semiconductors, such as BiErWO₆ (Di *et al.*, 2014), Au-Bi₂S₃ (Du and Luan, 2012), and BiNbO₄ (Manna *et al.*, 2014), is one of the optimal choices for its feasibility of constructing Z-scheme heterojunction with g-C₃N₄. Bismuth oxyhalide (BiOX), which is a kind of the layered ternary oxide semiconductors, has arisen much attention due to its high-photocatalytic efficiency for eliminating toxic textile dyes and other organic pollutants (Zhai *et al.*, 2013). Based on the recent reports, the BiOX compound like BiOCl is more effective than TiO₂ for methyl orange (MO) degradation under UV light illumination. However, BiOCl can only use the photons in the ultraviolet region (3% of the solar energy) and the rapid recombination of photogenerated charge carriers considerably restricts its quantum efficiency. Therefore, taking the advantages of pure BiOCl and g-C₃N₄ to construct the heterojunction structure can be a feasible way to improve the visible-light response and charge separation efficiency simultaneously.

In this work, considering the suitable conduction and valence bands level between BiOCl and g-C₃N₄, a novel visible-light driven g-C₃N₄/BiOCl heterojunction photocatalyst was designed and synthesized. The schematic formation process of 2D g-C₃N₄/BiOCl heterojunctions is shown in Figure 1.

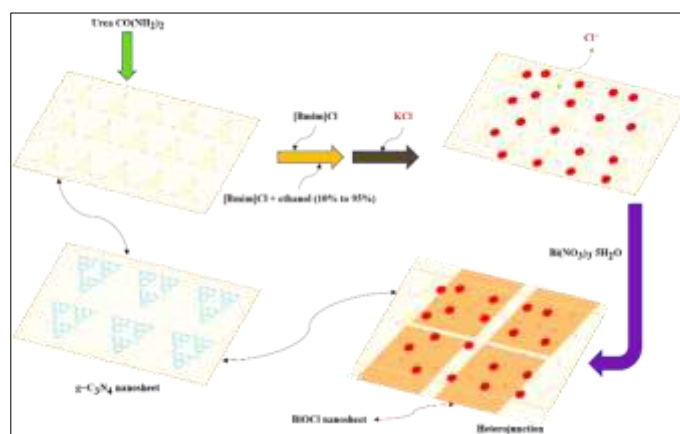


Figure 1 Schematic demonstration of the formation process for 2D g-C₃N₄/BiOCl heterojunctions in mixed polar solvent.

Materials and Methods

Chemicals and Reagents

Urea (CH₄N₂O) was purchased from Aladdin Industrial Corporation, Shanghai, China. Bismuth(III) nitrate pentahydrate was purchased from Tianjin Chemical Reagent Technology Co. Ltd. Tianjin, China. Potassium Chloride (KCl) was purchased from Tianjin Kermel Chemical Reagent Co. Ltd. Tianjin, China. The ionic liquid 1-butyl-3-methyl imidazolium chloride [Bmim]Cl was purchased from Shanghai Macklin Biotech Chemical Co. Ltd., Shanghai, China. Ethanol (EtOH) was purchased from Rionlon Bohua Pharmaceutical Chemical Co. Ltd. Tianjin, China. All chemicals were of analytical grade and used directly without further purification. Deionized water was used throughout all the experiments.

Synthesis of g-C₃N₄/BiOCl/Heterojunctions

The pristine g-C₃N₄ was prepared by the thermal polymerization of urea (Kang *et al.*, 2013). Briefly, 20 g of urea was put into a porcelain crucible with a cover to prevent the

sublimation of urea, and then heated at 510 °C for 4 h with a ramping rate of 2.5 °C min⁻¹ in a muffle furnace. The naturally-cooled resulting yellow product was ground to obtain a powder sample. Moreover, to prepare the carbon nitride product with broken hydrogen bonds, the pristine g-C₃N₄ was annealed at 580 °C for 2 h with a ramping rate of 5 °C min⁻¹ in a tube furnace under nitrogen atmosphere.

The samples of g-C₃N₄/BiOCl composites were synthesized using different ratios of solvents between water ($\sigma \leq 10^{-8} \Omega \text{ cm}^{-1}$) and ethanol. Different samples with solvent ratio using 10%-95% ethanol for the g-CN/BiOCl-1, 100 mL of 10% EtOH solution containing 1 mmol of ionic liquid (1-butyl-3-methyl imidazolium chloride) was sonicated for half an hour and then further stirred another 2 h to obtain a uniform suspension. After that, 0.75 g of KCl was dissolved in 50 mL of deionized water under sonication for half an hour. The ionic liquid solution was added into KCl solution and it was stirred for another half hour. Next, 4.85 g Bi(NO₃)₃.5H₂O was dissolved in 50 mL of deionized water, ultrasonicated for 0.5 h, then stirred on a magnetic stirrer for 2 h and added into the above solution dropwise with the flow rate at 2.5 mLmin⁻¹ under stirring. The heterogeneous solution was precipitated using 3-4 mL of 25% aqueous NH₃ solution and pH of the mixture was maintained at 2.0 and stirred continuously for another 15 h to get suspension of g-C₃N₄/BiOCl. Then, the resulting suspension was collected by filtration and washed five times with ethanol and water for complete removal of undesirable water-soluble products. Finally, solid powder sample was obtained by drying at 60 °C in an oven for overnight. A series of samples were prepared using same procedure by varying the ethanol compositions of 25%, 50%, 75%, and 95% which are noted as CN/BiOCl-X (X=1,2,3,4 and 5).

Characterization

The crystal phases of the material was analyzed using powder X-ray diffractometer (XRD) at a scanning rate of 5 ° min⁻¹. The surface morphology of as-synthesized samples was observed with a field emission scanning electron microscope (FE-SEM) (JEOL JSM-7001F) equipped with an energy-dispersive X-ray spectroscopy (EDX) operated at an acceleration voltage of 10 kV. The morphology and structure of the synthesized samples were further examined by the transmission electron microscopy (TEM). Fourier transform infrared spectroscopy (FTIR) was measured for functional group estimation using a Nicolet-560F Fourier transform infrared spectrometer. The diffuse reflectance spectrum (DRS) was recorded with a UV-Vis spectrophotometer (U-3010, Hitachi) equipped with an integrating sphere, using BaSO₄ as the reference.

Photocatalytic Activity

In brief, 20 mg of photocatalyst was dispersed into 30 mL of 10 mgL⁻¹ RhB. Prior to the irradiation, the suspension was magnetically stirred for 30 min in the dark to ensure the adsorption-desorption equilibrium. Then 2.0 mL suspension was collected and centrifuged and the dye concentration was analyzed with a UV-Vis spectrophotometer (Hitachi-3900) at 553 nm for RhB.

Results and Discussion

Morphology and Structure of g-C₃N₄/BiOCl Heterojunctions

X-ray power diffraction peaks were analyzed to investigate phase structures of pure BiOCl, g-C₃N₄ and g-C₃N₄/BiOCl composites as shown in Figure 2a. The diffraction peaks of synthesized samples appear at 2 θ values which match with (hkl) values according to JCPDS card No. 85-0861 for g-C₃N₄ and No. 06-0249 for BiOCl. However, the typical (002) plane peak of g-C₃N₄ does not appear in the composites, probably low concentration and relatively low diffraction intensity of g-C₃N₄ in the g-C₃N₄/BiOCl (Xiong *et al.*, 2011). The results suggest that the coupling of BiOCl and g-C₃N₄ should take place between (001) plane of BiOCl and (002) plane of g-C₃N₄. The mutual

covering of BiOCl (001) plane and g-C₃N₄ (002) plane would lead to the decrease in the diffraction intensity. The weak peak around 27° (2θ) is a characteristic interlayer stacking peak of aromatic system, which indexes the (002) plane of graphitic materials. No impurity was observed from the patterns. Moreover, sharp and clear diffraction peaks illustrate that all composites have good crystallinity.

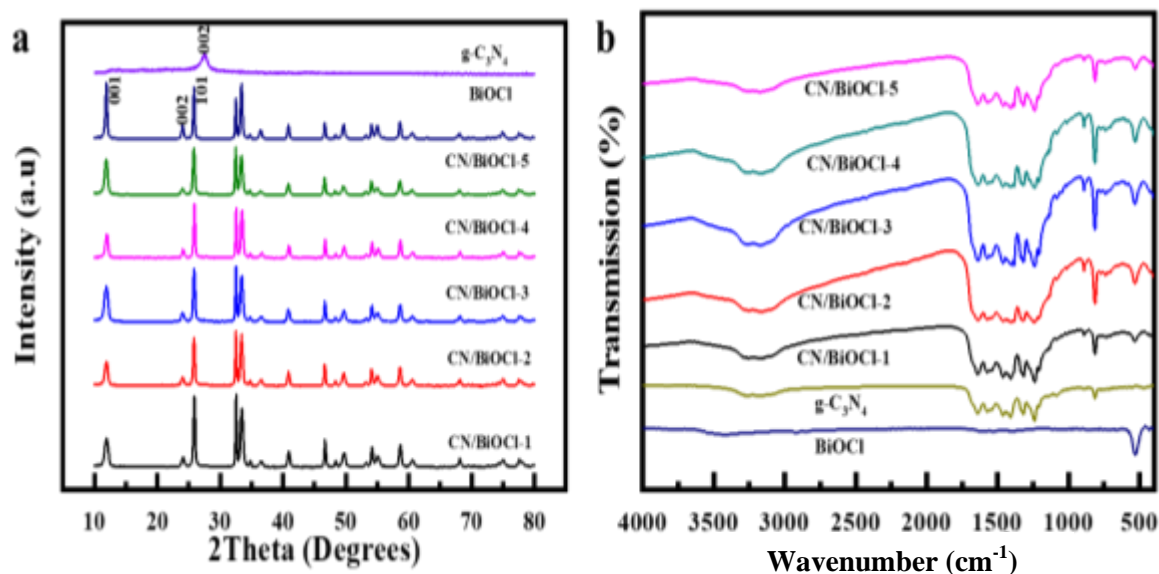


Figure 2 (a) XRD patterns and (b) FT IR spectra of pure g-C₃N₄, BiOCl and 2D g-C₃N₄/BiOCl heterojunctions prepared in different solvents

The results of FT IR spectra analysis of the composite samples are displayed in Figure 2b. In the composites, the broad absorption band at 3209 cm⁻¹ is attributed to the stretching vibration mode of N-H on the g-C₃N₄ surface due to the surface defective sites. Additionally, the broad absorption band at 1644, 1577, 1465, 1402, and 1242 cm⁻¹ can be assigned to the typical skeletal stretching modes of C-N heterocycles and tris-s-triazine. These absorption peaks indicate the maintenance of g-C₃N₄ basic structure after hybridization. With regard to the composites g-C₃N₄/BiOCl-1 to 5, the sharp peak at 512 cm⁻¹ in the spectrum can be assigned to the stretching vibration mode of Bi-O in a tetragonal phase of the BiOCl crystal. Moreover, a characteristic breathing mode of s-triazine at 813 cm⁻¹ is observed. To sum up, the coupling of composites is attributed to the intense interaction between g-C₃N₄ and BiOCl phases with the increase of ethanol concentration.

Figure 3 shows the SEM images of the as-prepared samples in different solvents. It is clear that the composites consist of a large number of irregular nanosheets. Although the morphology of as-prepared samples is uniform, the separated bulk nanosheets provide more active sites for the interaction with pollutant molecules. In fact, by using the lower concentration of ethanol, the structures of well-defined flake-like nanosheets with round corners can be observed. Moreover, one can see that with the increase of the ethanol concentration, the sample size becomes larger. It can be concluded that there are distinct differences in platelet shape suggesting that the two-dimensional bulky flake-like nanosheets morphology can be adjusted using different solvent ratios by different attractive forces in the reaction system (Ye *et al.*, 2013; Xiong *et al.*, 2011). As shown in Figure 3g, several g-C₃N₄ spread the surface of BiOCl nanosheets uniformly. The dense structure can be attributed to the localization of electrons and stronger binding between the layers. For pure BiOCl, the flower-shape irregular nanosheets were observed as shown in Figure 3b. After combining with two composites, as-prepared samples changed to bulky and smooth flake-like nanosheets.

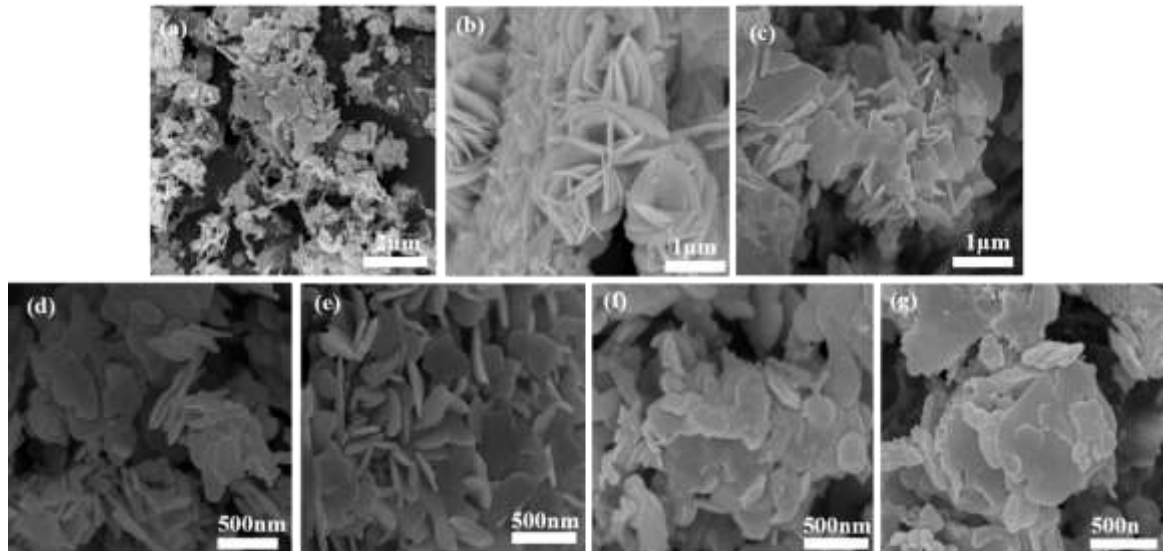


Figure 3 SEM images of 2D $g\text{-C}_3\text{N}_4/\text{BiOCl}$ heterojunctions: (a) pure $g\text{-C}_3\text{N}_4$, (b) pure BiOCl , (c) $g\text{-C}_3\text{N}_4/\text{BiOCl}$ -1, (d) $g\text{-C}_3\text{N}_4/\text{BiOCl}$ -2, (e) $g\text{-C}_3\text{N}_4/\text{BiOCl}$ -3, (f) $g\text{-C}_3\text{N}_4/\text{BiOCl}$ -4 and (g) $g\text{-C}_3\text{N}_4/\text{BiOCl}$ -5

Figure 4 shows the TEM images of several composites with polycrystalline structures and agglomerate. All composites consisting of numerous uniform nanosheets and tiny nanosheets of $g\text{-C}_3\text{N}_4$, which can be seen on the surface of BiOCl . Due to the presence of tiny nanosheets in the composites, the photocatalytic activity of composites can be enhancing under visible-light irradiation based on more active sites.

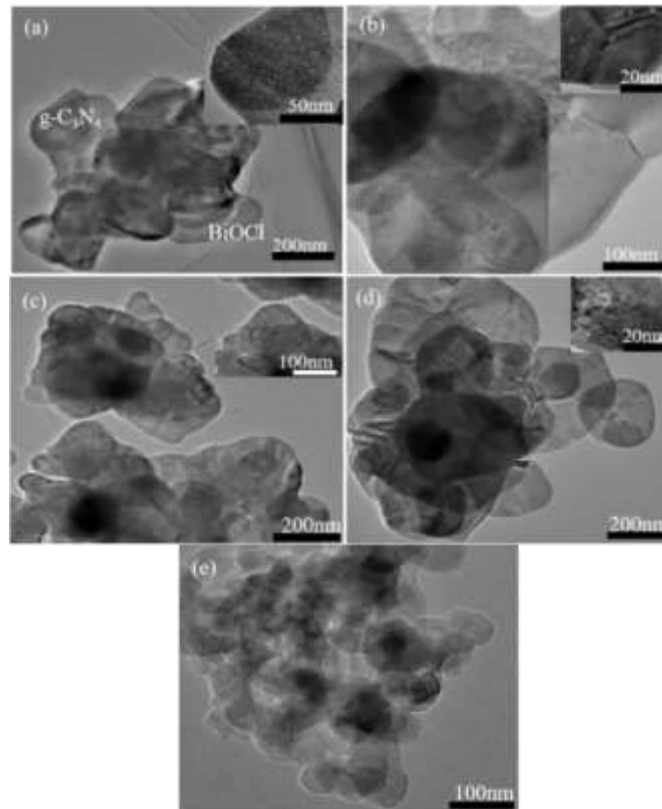


Figure 4 TEM images of as-prepared $g\text{-C}_3\text{N}_4/\text{BiOCl}$ heterojunctions: (a) $g\text{-C}_3\text{N}_4/\text{BiOCl}$ -1, (b) $g\text{-C}_3\text{N}_4/\text{BiOCl}$ -2, (c) $g\text{-C}_3\text{N}_4/\text{BiOCl}$ -3, (d) $g\text{-C}_3\text{N}_4/\text{BiOCl}$ -4 and (e) $g\text{-C}_3\text{N}_4/\text{BiOCl}$ -5

Optical Properties of g-C₃N₄/BiOCl Heterojunctions

The optical absorption and energy band feature of the semiconductors are important for determining its photocatalytic performance. The DRS of the as-prepared samples is shown in Figure 5a. It can be seen that the main absorption edge of pure BiOCl is located around 360 nm, while pure g-C₃N₄ can absorb the light from UV through the visible range up to 462 nm. The g-C₃N₄/BiOCl heterojunction (1 to 5) exhibit the adsorption edges in the visible-light absorption region, indicating the combination of the optical property of g-C₃N₄ with that of BiOCl. As the concentration of ethanol solvent increases to 75%, the absorption wavelength of g-C₃N₄/BiOCl-4 heterojunction at 468 nm for g-C₃N₄ increases, while that at 405 nm for BiOCl simultaneously decreases. Moreover, the absorption edge of g-C₃N₄/BiOCl samples exhibits a red shift in comparison with those of pure g-C₃N₄ and BiOCl with increasing the ethanol concentration. The band gap energy of semiconductors can be calculated approximately based on the following equation:

$$\alpha h\nu = A(h\nu - E_g)^{n/2} \quad (1)$$

Where α , h , ν , E_g and A are the absorption coefficient, Planck's constant, light frequency, band gap energy and constant respectively; n is determined by the type of optical transition of a semiconductor ($n=1$ for direct transition and $n=4$ for indirect transition) (Jiang *et al.*, 2012; Xiao *et al.*, 2012). As can be seen in Figure 5b, E_g values of pure g-C₃N₄ and BiOCl are estimated to be 2.65 eV and 3.44 eV, respectively. The band gaps of g-C₃N₄/BiOCl composites gradually decrease with increasing the ethanol ratio to 95%, i.e. changing from 2.70 eV to 2.65 eV. Then, the band gaps of BiOCl in g-C₃N₄/BiOCl composites gradually decrease with increasing the ethanol solvent ratio up to 95%, changing from 3.44 eV to 3.06 eV determined from a plot of $(\alpha h\nu)^{1/2}$ versus $h\nu$. From these results, it can be deduced that all of the g-C₃N₄/BiOCl-1 to 5 have suitable band gaps to be activated by visible-light for photocatalytic decomposition of organic contaminants

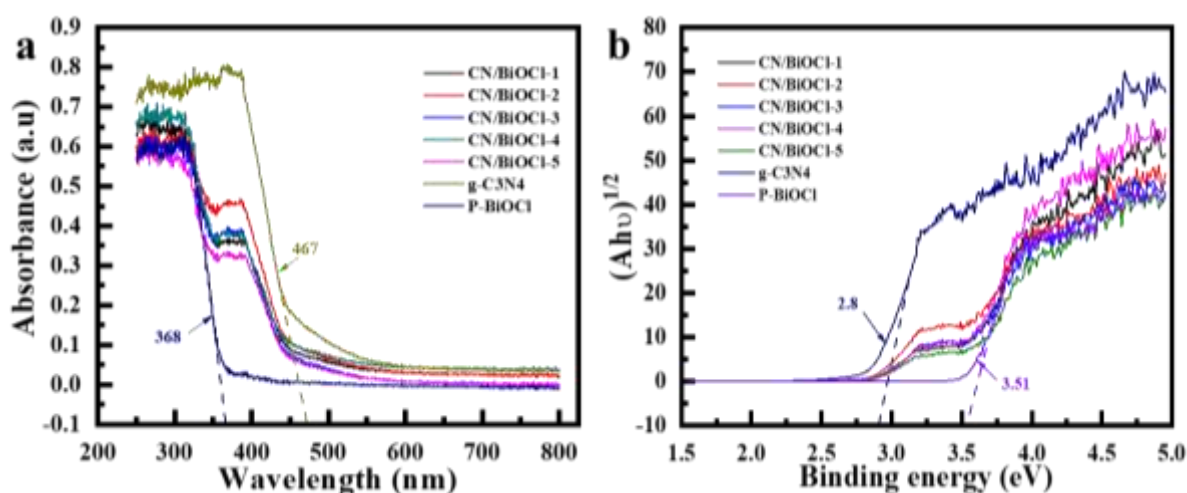


Figure 5 (a) UV-Vis diffuse reflectance spectra (b) Band gap plot of $(\alpha h\nu)^{1/2}$ vs. $h\nu$ (eV) curves for pure g-C₃N₄, g-C₃N₄/BiOCl samples and BiOCl

The band edge position of conduction band (CB) and valence band (VB) for a semiconductor can be calculated according to the following theoretical empirical formulae (Zhang *et al.*, 2005),

$$E_{CB} = \chi - E^e - 0.5E_g \quad (2)$$

$$E_{VB} = E_{CB} + E_g \quad (3)$$

where E_{CB} is the conduction band (CB) edge potential; χ is the absolute electronegativity of the constituent atoms, expressed as the arithmetic mean of the atomic electron affinity and the first ionization energy; E^e is the energy of free electrons on the hydrogen scale (~ 4.5 eV); E_g is the band gap energy of the semiconductor; E_{VB} is the valence band (VB) edge potential. The absolute electronegativity values for BiOCl and g-C₃N₄ are 6.36 and 4.73 eV, respectively. As can be seen in Figure 5b for CN/BiOCl-4, g-C₃N₄ has an electronic structure with an appropriate band gap energy of 2.65 eV, corresponding to an optical wavelength of 468 nm. The conduction band and valence band values of g-C₃N₄ in CN/BiOCl-4 are at -1.09 eV and 1.56 eV, respectively. BiOCl has an electronic structure with an appropriate band gap energy of 3.06 eV, corresponding to an optical wavelength of 468 nm. Then, the conduction band and valence band edge values of BiOCl in composite CN/BiOCl-4 are 0.33 eV and 3.39 eV, respectively, as can be seen in Table 2. These electronic structures of g-C₃N₄ and BiOCl possess good photo-response, which can be easily excited thus engendering the photogenerated electron-hole pairs under visible-light irradiation. The layer structure of g-C₃N₄ is beneficial for the transformation of the electron to BiOCl in CN/BiOCl-4. Indeed, their layered structure feature endows those self-built internal static electric fields, which can improve the effective separation of the photo induced electron-hole pair.

Table 2 Absolute Electronegativity, Calculated CB Edge, Calculated VB Position and Band Gap Energy for C₃N₄ and BiOCl in g-C₃N₄/BiOCl Heterojunction at the Point of Zero Charge

Semiconductors	Absolute electronegativity (χ) (eV)	Calculated CB position (eV)	Calculated VB position (eV)	Band gap energy, E_g (eV)
g-C ₃ N ₄	4.73	-1.09	1.56	2.65
BiOCl	6.36	0.33	3.39	3.06

Photocatalytic Performance of g-C₃N₄/BiOCl Heterojunctions

To prove the photocatalytic activity of g-C₃N₄/BiOCl heterojunctions, RhB was chosen as the target organic dye pollutant. The characteristic absorption band of RhB at 553 nm is employed to monitor the degradation process under visible-light irradiation. As shown in Figure 6a, RhB self-photolysis without catalyst is not observable, indicating that RhB is stable under visible-light irradiation. For composites, the photocatalytic performance is gradually enhanced with the ethanol ratio increases from 10% to 75% in the presence of ionic liquid. The catalytic efficiency can achieve ~ 100 % removal within 1 h. Furthermore, the ethanol ratio was increased to 95% ethanol, contrarily leading to the increase of photocatalytic degradation activity. It can be seen that both g-C₃N₄ and BiOCl behave the important function in g-C₃N₄/BiOCl for improving the photocatalytic efficiency at 75% of ethanol ratio. The g-C₃N₄/BiOCl heterojunctions are 2D-2D layered composites, which enhance the photocatalytic performances due to the increased contact surface area and charge transfer rate. Furthermore, compared with other 2D material-based composites (i.e. 0D-2D and 1D-2D composites), 2D-2D layered nanosheets composite can achieve a solid construction due to the large contact surface area between two sheets, and exhibit greater stability than 0D-2D and 1D-2D composites (Low *et al.*, 2014).

In order to understand the reaction kinetics of dye degradation, the pseudo-first-order rate constant was expressed according to the following equation:

$$-\ln \frac{C}{C_0} = kt$$

In the above equation, k is the kinetic constant. C_0 and C are the initial and final concentration of RhB in solution at time 0 and t , respectively. $g\text{-C}_3\text{N}_4/\text{BiOCl}$ composites exhibit the higher rate constants than pure $g\text{-C}_3\text{N}_4$ and BiOCl . It can be seen that the rate constant values of $g\text{-C}_3\text{N}_4/\text{BiOCl}$ composites changed distinctly (Figure 6 b). The maximum value of k is 0.046 min^{-1} for CN/BiOCl -4, which is three times as high as that of pure BiOCl under visible-light illumination over RhB. Therefore, the modification of $g\text{-C}_3\text{N}_4$ with BiOCl could effectively enhance the photocatalytic activity by using high polar solvent ratio. Moreover, the kinetic constant values of as-prepared $g\text{-C}_3\text{N}_4/\text{BiOCl}$ (1 to 5) follows the decreasing rate of CN/BiOCl -4 > CN/BiOCl -5 > CN/BiOCl -3 > CN/BiOCl -1 > CN/BiOCl -2 > BiOCl > $g\text{-C}_3\text{N}_4$.

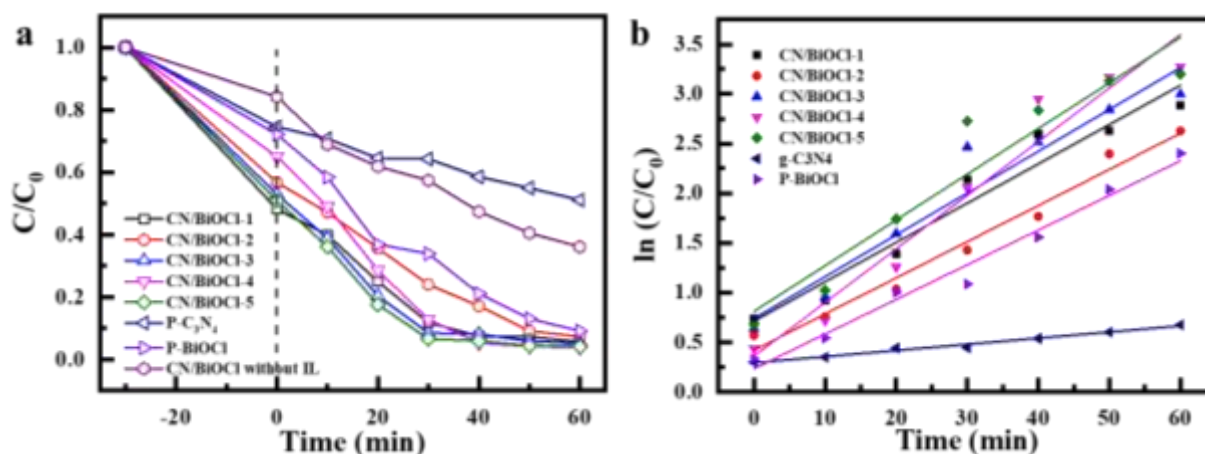


Figure 6 Photocatalytic activity of (a) RhB dye degradation; (b) pseudo-first-order kinetics plot of for RhB with pure $g\text{-C}_3\text{N}_4$, pure BiOCl , and $g\text{-C}_3\text{N}_4/\text{BiOCl}$ composites under visible-light irradiation

Photocatalytic mechanism of $g\text{-C}_3\text{N}_4/\text{BiOCl}$ -4 heterojunction

The enhancement of the photocatalytic activity of the $g\text{-C}_3\text{N}_4/\text{BiOCl}$ -4 composite is mainly attributed to the effective separation of the photogenerated electron-hole pairs. As shown in Figure 7, both $g\text{-C}_3\text{N}_4$ and BiOCl are easily excited thus engendering the photogenerated electron-hole pairs. Unlike the traditional model, the Z-scheme mechanism photocatalysts retain stronger redox abilities, contributing to the improvement of photocatalytic performance.

$g\text{-C}_3\text{N}_4$ has an electronic structure with an appropriate band gap of 2.65 eV, corresponding to an optical wavelength of 468 nm. The estimated CB and VB of $g\text{-C}_3\text{N}_4$ material are -1.09 eV and 1.56 eV, respectively. The CB and VB edge potentials of BiOCl were at 0.33 eV and 3.39 eV. Here, the CB value of $g\text{-C}_3\text{N}_4$ (-1.06 eV) is more negative than that of BiOCl (0.18 eV), while the VB of BiOCl (3.54 eV) is more positive than that of $g\text{-C}_3\text{N}_4$ (1.52 eV). The $g\text{-C}_3\text{N}_4$ and BiOCl semiconductors belong to overlapping band potentials, suggesting that the band potential of $g\text{-C}_3\text{N}_4$ and BiOCl can be matched to fabricate the effective heterojunction. In general, the charge separation occurs in a heterojunction with different band gaps and edge positions. In this study, the dissolved O_2 in the aerated solutions act as an electron acceptor and the E_{CB} of $g\text{-C}_3\text{N}_4$ is more negative than the standard redox potential of $E(\text{O}_2/\cdot\text{O}_2^-)$. Furthermore, the VB of $g\text{-C}_3\text{N}_4$ and CB of BiOCl are close to each other. Therefore, the photo-excited electrons in the CB of BiOCl rapidly transfer to VB of $g\text{-C}_3\text{N}_4$, leading to the combination of photogenerated electrons in the CB of BiOCl with photogenerated holes in the VB of $g\text{-C}_3\text{N}_4$. Then, these accumulating electrons in the CB of $g\text{-C}_3\text{N}_4$ and holes in the VB of BiOCl participate in the dye degradation. Consequently, the more negative potentiated electrons in the CB of $g\text{-C}_3\text{N}_4$ reduce the molecular oxygen to yield $\cdot\text{O}_2^-$, which induces the RhB degradation. Meanwhile, the more positive potentiated holes in the VB of BiOCl produce active $\cdot\text{OH}$ with powerful oxidation. In addition, the holes in the VB of BiOCl can

directly oxidize the organic dyes. Therefore, the charge transfers of the g-C₃N₄/BiOCl-4 composite may follow a direct Z-scheme route, which can improve the photogenerated electron-hole pair separation efficiency and enhance the photocatalytic activity for the degradation of organic pollutants.

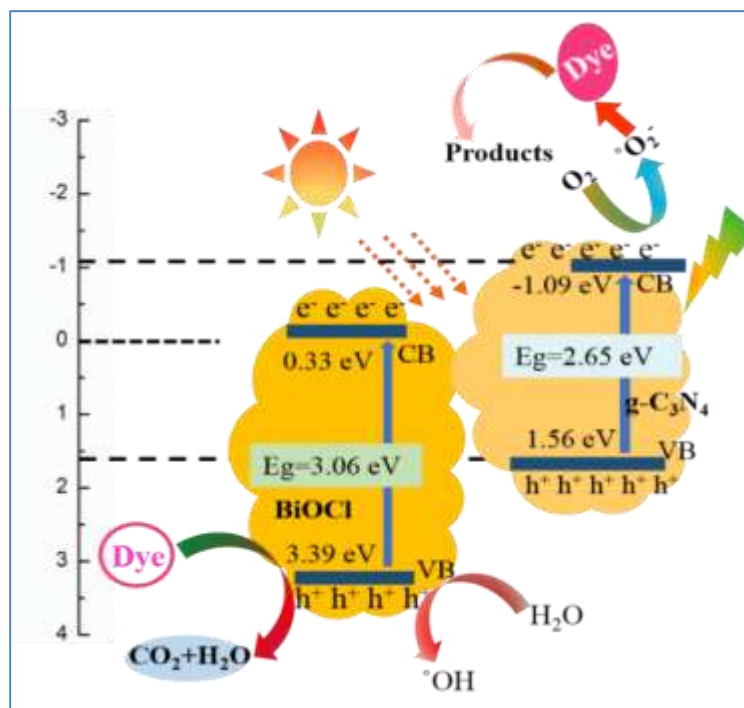


Figure 7 Schematic illustration of the photocatalytic mechanism for the dye degradation by using g-C₃N₄/BiOCl-4 heterojunction under visible-light.

Conclusion

The novel 2D g-C₃N₄/BiOCl heterojunctions were prepared by using a one-pot ethanol-assisted solvothermal method in the presence of ionic liquid [Bmim]Cl. The morphology characterization indicated that the g-C₃N₄ nanosheet covers the surface of flake-like BiOCl uniformly and the heterostructures formed when the ethanol ratio is in the range of 10-95%. Their band gap energies were lower than pure g-C₃N₄ and BiOCl as the ethanol ratio increased. The as-synthesized g-C₃N₄/BiOCl heterostructures display enhanced degradation performance in comparison with pure g-C₃N₄ and BiOCl, which can be attributed to the favorable optical property and suitable energy band gap potential. Among all the samples, CN/BiOCl-4 showed the highest photocatalytic activity. The heterojunction formed between g-C₃N₄ and BiOCl enhanced electron-hole recombination and photocatalytic activity. These results indicated that the g-C₃N₄/BiOCl nanosheet is a promising candidate photocatalyst for wastewater treatment and textile dyes degradation due to its enhanced photocatalysis properties.

Acknowledgements

The authors thank the financial support from the National Natural Science Foundation of China (21621004, 91534126), National Science Fund for Distinguished Young Scholars (21125627), Natural Science Foundation of Tianjin (18JCYBJC21000) and Program of Introducing Talents of Discipline to Universities (B06006). Also, the authors would like to express their profound gratitude to the Department of Higher Education, Ministry of Education, Yangon, Myanmar, for provision of opportunity to Myanmar Academy of Arts and Science for allowing to present this paper.

References

- Akhavan, O. and Ghaderi, E. (2013). "Differentiation of Human Neural Stem Cells on Graphene/TiO₂ Heterojunction for Differentiation into Neurons". *Nanoscale*, vol. 5, pp. 10316-10326
- Cai, L. (2015). "Enhanced Visible Light Photocatalytic Activity of BiOCl by Compositing with g-C₃N₄". *Mater. Research Innovations*, vol.19(5), pp. 392-396
- Di, J., Xia, J., Yin, S., Xu, H., Xu, L., Xu, Y., He, M. and Li, H. (2014). "Preparation of Sphere-Like g-C₃N₄/BiOI Photocatalysts via Reactable Ionic Liquid for Visible-Light-Driven Photocatalytic Degradation of Pollutants". *J. Mater. Chem. A*, vol.2, pp. 5340-5351
- Du, H.Y. and Luan, J. F. (2012). "Synthesis, Characterization and Photocatalytic Activity of New Photocatalyst CdBiYO₄". *Solid State Sci.*, vol.14, pp. 1295-1305
- Fujishima, A., Tata, N. R. and Donald, A. T. (2000). "Titanium Dioxide Photocatalysis". *J. Photochemistry and Photobiology C*, vol. 1(1), pp. 1-21
- Hou, Y. F., Liu, S. J., Zhang, J. H., Cheng, X., Wang, Y. (2014). "Facile Hydrothermal Synthesis of TiO₂-Bi₂WO₆ Hollow Superstructures with Excellent Photocatalysis and Recycle Properties". *Dalton Trans.*, vol. 43, pp. 1025-1031
- Jiang, J., Zhao, K., Xiao, X. Y. and Zhang, L. Z. (2012). "Synthesis and Facet-Dependent Photoreactivity of BiOCl Single-Crystalline Nanosheets". *J. Am. Chem. Soc.*, vol.134(10), pp. 4473-4476
- Kang, Y. Y., Yang, Y. Q., Yin, L. C., Kang, X. D., Wang, L. Z., Liu, G., Cheng, H. M. (2013). "Selective Breaking of Hydrogen Bonds of Layered Carbon Nitride for Visible Light Photocatalysis". *Adv. Mater.*, vol.28, pp. 6471-6477
- Low, J., Cao, S., Yu, J., Wageh, S. (2014). "Two-Dimensional Layered Composite Photocatalysts". *Chem. Commun.*, vol.50(74) pp. 10768-10777
- Manna, G., Bose, R. and Pradhan, N. (2014). "Photocatalytic Au-Bi₂S₃ Heterostructures. *J. Angew. Chem. Int. Ed.*, vol.53(26), pp. 6743-6746
- Regan, B. O. and Gratzel, M. (1991). "Low-Cost High Efficiency Solar Cell Based on Dye-Sensitized Colloidal TiO₂ Films". *Nature*, vol.353, pp. 737-740
- Sharma, I.D., Tripathi, G.K., Sharma, V.K., Tripathi, S. N., Kurchania, R., Kant, C., Sharma, A.K. and Sain, K.K. (2015). "One-pot Synthesis of Three Bismuth Oxyhalides (BiOCl, BiOBr, BiOI) and Their Photocatalytic Properties in Three Different Exposure Conditions". *Cogent Chem.*, vol. 1(1), pp. 1-15
- Wang, X. C., Maeda, K., Thomas, A., Takanabe, K., Xin, G., Carlsson, J. M., Domen, K. and Antonietti, M. (2009). "A Metal-Free Polymeric Photocatalyst for Hydrogen Production from Water Under Visible Light". *Nature Materials*, vol.8, pp.76-80
- Weng, S. X., Chen, B., Xie, L., Zheng, Z. and Liu, P. (2013). "Facile *in Situ* Synthesis of a Bi/BiOCl Nanocomposites with High Photocatalytic Activity". *J. Mater. Chem. A*, vol.1, pp. 3068-3075
- Xiao, X., Hao, R., Liang, M., Zuo, X. X., Nan, J. M., Li, L. S. and Zhang, W. D. (2012). "One Pot Solvothermal Synthesis of Three-Dimensional (3D) BiOI/BiOCl Composites with Enhanced Visible-Light Photocatalytic Activities for the Degradation of Bisphenol-A". *J. Hazard. Mater.*, vol. 233, pp. 122-130
- Xiong, J. Y., Cheng, G., Li, G. F., Qin, F. and Chen, R. (2011). "Well-Crystallized Square-like 2D BiOCl Nanoplates: Mannitol-Assisted Hydrothermal Synthesis and Improved Visible-Light-Driven Photocatalytic Performance". *RSC Adv.*, vol.1, pp. 1542-1553
- Yamasita, D., Takata, T., Michikazu, H., Junko, N. K. and Domen, K. (2004). "Recent Progress of Visible-Light-Driven Heterogeneous Photocatalyst for Overall Water Splitting". *Solid State Ionics*, vol.172, pp.591-595
- Yan, S. C., Li, Z. S. and Zou, Z. G. (2009). "Photodegradation Performance of g-C₃N₄ Fabricated by Directly Heating Melamine". *Langmuir Article*, vol.25(17), pp. 10397-10401
- Ye, L., Liu, J. Y., Jiang, Z., Peng, T. Y. and Zan, L. (2013). "Facets Coupling of BiOBr-g-C₃N₄ Composite Photocatalyst for Enhanced Visible Light-Driven Photocatalytic Activity". *Appl. Catal. B*, vol.142-143, pp. 1-7
- Zhai, H. F., Li, A. D., Kong, J. Z., Li, X. F., Zhao, J., Guo, B. L., Yin, J., Li, Z. S. and Wu, D. (2013). "Preparation and Visible Light Photocatalytic Properties of BiNbO₄ and BiTaO₄ by a Citrate Method". *J. Solid State Chem.*, vol.202, pp. 6-14
- Zhang, K. L., Liu, C. M., Haung, F. Q., Zheng, C. and Wang, W. D. (2006) "Study of the Electronic Structure and Photocatalytic Activity of the BiOCl Photocatalyst". *Appl. Catalysis B. Environ.*, vol.68(3-4), pp.125-129
- Zhang, X. T., Sato O., Taguchi, M., Einaga, Y., Murakami, T. and Fukushima, A. (2005). "Self-Cleaning Particle Coating with Antireflection Properties". *Chem. Mater.*, vol.17(3), pp. 696-700